HHS Public Access

Author manuscript

Nat Neurosci. Author manuscript; available in PMC 2013 March 01.

Published in final edited form as:

Nat Neurosci. 2012 September ; 15(9): 1236–1244. doi:10.1038/nn.3173.

Paradoxical Contribution of SK3 and GIRK Channels to the Activation of Mouse Vomeronasal Organ

SangSeong Kim[1], **Limei Ma**[1], **Kristi L. Jensen**[1], **Michelle M. Kim**[2], **Chris T. Bond**[3], **John P. Adelman**[3], and **C. Ron Yu**[1,4,*]

[1]Stowers Institute for Medical Research, Kansas City, MO 64110

[2]Department of Biochemistry and Molecular Biophysics, College of Physicians and Surgeons, Columbia University, New York, NY 10032

[3]Vollum Institute, Oregon Health & Science University, Portland, OR 97239

[4]Department of Anatomy and Cell Biology, Kansas University Medical Center, Kansas City, KS 66160

Abstract

The vomeronasal organ (VNO) plays an essential role in intraspecies communication for terrestrial vertebrates. The ionic mechanisms of VNO activation remain unclear. We find that the calcium–activated potassium channel SK3 and G–protein activated potassium channel GIRK are part of an independent pathway for VNO activation. In slice preparations, the potassium channels attenuate inward currents carried by TRPC2 and calcium–activated chloride channels (CACCs). In intact tissue preparations, paradoxically, the potassium channels enhance urine–evoked inward currents. This discrepancy results from the loss of a high concentration of lumenal potassium, which enables the influx of potassium ions to depolarize the VNO neurons *in vivo*. *SK3*$^{-/-}$ and *GIRK1*$^{-/-}$ mice show deficits in both mating and aggressive behaviors and deficiency in *SK3*$^{-/-}$ is exacerbated by TRPC2 knockout. Our results suggest a model of VNO activation that is mediated by TRPC2, CACCs and two potassium channels, all contributing to the *in vivo* depolarization of VNO neurons.

INTRODUCTION

Sensory systems have evolved to represent salient features of an organism's environment. In terrestrial vertebrates, the perception of olfactory cues is carried out by two anatomically and functionally distinct olfactory sensory systems: the vomeronasal organ (VNO) and the main olfactory epithelium (MOE). The MOE provides a broad sampling of the olfactory world and elicits a large number of cognitive and behavioral responses. In contrast, the VNO

*Corresponding author: cry@stowers.org.

Author Contributions

S.K. and C.R.Y. performed electrophysiology experiments and data analyses; L.M. and C.R.Y. perform histology experiments; L.M. prepared mice used in the studies; K.L.J., M.M.K. and C.R.Y. performed behavior analyses; C.T.B. and J.P.A. contributed critical reagent; C.R.Y. wrote the manuscript with the inputs from S.K., L.M., J.P.A. and K.L.J.

detects a distinct set of chemical cues, including pheromones that provide information about the sexual, social, and reproductive status of other members of the species. Pheromones recognized by the VNO trigger a restricted repertoire of innate behaviors and neuroendocrine responses such as mating rituals and territorial aggression [1].

The two systems have evolved independently to accommodate the unique requirements of the two olfactory senses. The main olfactory system primarily detects volatile, air–borne chemicals. Although the VNO may also respond to volatile odors, it mainly detects non–volatile chemicals including proteins and peptides [2]. The vomeronasal system is strongly activated when the nose is in close contact with the pheromone sources, whereupon an active pumping mechanism is used to bring external cues into the VNO [3]. Thus, the VNO neurons are likely to be exposed to various ionic environments where pheromones are found.

In the VNO, three distinct families of G–protein coupled receptors, V1Rs, V2Rs and the FPRs, are found to be expressed by the sensory neurons [4–10]. Receptor occupancy activates phospholipase C (PLC) and results in elevating the levels of inositol 1,4,5–trisphosphate (IP3), diacylglycerol (DAG) and their metabolites [11–14]. These events are thought to lead to the activation of TRPC2, a member of the TRP superfamily of non–selective cation channels [15–17]. Genetic knockout of the TRPC2 channel results in a significant loss of pheromone–triggered responses in VNO neurons and aberrant innate behaviors [18–20]. Recent studies have shown that TRPC2 is not the sole ion channel mediating urine–evoked currents. Electrophysiological studies in hamster and mouse have identified a Ca^{2+}–activated non–selective cation current in the VNO [21, 22]. A Ca^{2+}–activated Cl^- current has been identified in mouse to mediate urine–evoked inward current [23]. We have shown that the activation of the Cl^- conductance is triggered by both Ca^{2+} entry through the TRPC2 channel and Ca^{2+} release from the intracellular stores [24].

In this study, we investigate the contribution of K^+ channels in VNO signaling. We demonstrate that a significant contribution to the urine–evoked response derives from the activation of a small conductance Ca^{2+}–activated K^+ channel, SK3, as well as a G–protein activated inwardly rectifying K^+ (GIRK) channel. We further show that the VNO mucus maintains an uncommon environment containing a high concentration of K^+. This creates a gradient that results in an influx of K^+ through the SK3 and GIRK channels in response to urine stimulation *in vivo*.

METHODS

Animals

Urine–evoked responses were obtained from 2–6 months old mice. 84 C57BL/6J, 15 $SK3^{T/T}$, 30 $TRPC2^{-/-}$ and 25 $GIRK1^{-/-}$ animals were used. Approximately equal numbers of male and female mice were used. Animals were maintained in the Lab Animal Service Facility of Stowers Institute at 12:12 light cycle, and provided with food and water *ad libitum*. Experimental protocols were approved by the Institutional Animal Care and Use Committee at Stowers Institute and in compliance with NIH Guide for Care and Use of Animals.

TRPC2$^{-/-}$, *SK3*$^{T/T}$ and *GIRK1*$^{-/-}$ mice were described previously [19, 27, 30]. To generate *SK3*$^{-/-}$ mice, homozygote *SK3*$^{T/T}$ mice were placed on doxycycline diet and pups were weaned to doxycycline feed. *GIRK1*$^{-/-}$ mice were obtained from Dr. Kevin Wickman and colleagues [30].

In Situ Hybridization

The hybridization buffer contained 50% formamide, 5X SSC, 1X Denhardts, 250 μg/ml yeast tRNA, 500 μg/ml herring sperm DNA, and 0.1% Tween–20. Probes specific for mouse *sk1*, *sk2* and *sk3* were synthesized from the 3' UTR of the respective genes using the DIG RNA labeling kit (Roche). In order to enhance sensitivity and reduce background, all antibody staining steps were performed in the presence of 0.1% Triton X–100, and the reaction was developed in buffer containing 0.1% Tween–20. Following alkaline phosphatase staining, the slides were coverslipped with Glycergel (DAKO) and viewed with Nomarski optics.

Immunofluorescent staining

Mouse VNO was dissected out and frozen in OCT Compound (Tissue–Tek). 12 μm coronal sections were collected on Superfrost slides (Fisher), fixed in 4% paraformaldehyde at 4°C, and washed three times in PT solution (0.1% Triton X–100 in PBS) at room temperature. The sections were incubated overnight with primary antibodies against different proteins in PTS (1% goat serum in PT) at 4°C. Rabbit anti–SK3 and rabbit anti–GIRK1 antibodies were purchased from Alomone Labs in Israel. Guinea pig anti–TRPC2 antibodies used in Fig. 2 were generated as described previously [19]. This particular batch of antibodies was lost. In subsequent stainings, rabbit anti–TRPC2 antibodies (a gift of Dr. Emily Liman) were used [15]. Secondary antibodies that include: FITC–conjugated donkey anti–rabbit, Cy3–conjugated donkey anti–rabbit secondary antibodies (Jackson Lab), Alexa 488–conjugated donkey anti–rabbit, Alexa 546–conjugated donkey anti–guinea pig antibodies (Molecular Probes). Co–staining for SK3 and TRPC2 was conducted by mixing the rabbit anti–SK3 and the guinea pig anti–TRPC2 antibodies together. We were not able to perform double staining with GIRK1 and TRPC2 because the guinea pig anti–TRPC2 antibodies were no longer available.

Electrophysiology

Urine Samples—Urine samples were collected from mature male and female animals using the free–catch method. The freshly collected urine samples were frozen at −80°C until use for up to 3 months. Equal volumes of male and female urine were mixed and diluted to 1:100 in Ringer solutions for stimulation.

Slice preparation—Mice were killed by rapid cervical dislocation after CO2 asphyxiation. The VNOs were dissected out into mouse artificial cerebrospinal fluid (mACSF) that was continuously aerated with 95% O_2 / 5% CO_2 and maintained at 4°C. The tissue was embedded in a gel composed of 4% low melting point agarose prepared in mACSF and mounted on a specimen holder of the VF–300 microtome sectioning system (Precisionary Instruments). Tissue samples were sectioned into 200 μm slices, which were then transferred to mACSF solution continuously aerated with 95% O_2 / 5% CO_2 at room

temperature. The composition of mACSF is (in mM): NaCl 125, KCl 2.5, $CaCl_2$ 2, $MgCl_2$ 1, $NaHCO_3$ 10, Na_2HPO_4 1.25, and Glucose (Dextrose) 10.

Patch Clamp Recordings—A VNO slice was placed in a recording chamber continuously superfused with oxygenated mACSF on an Olympus BX50WI upright microscope. An infrared DIC camera was used with a 40X objective to guide patch pipette to individual neurons. Patch clamp recording pipettes with resistance of 4–8 MΩ were fabricated using laser based P–2000 micropipette puller (Sutter Instrument).

Whole cell patch clamp—Recording was conducted using Multiclamp 700A amplifier (Molecular Device) with 10 KHz sampling rate and low–pass filtered at 100 Hz for voltage clamp experiments and 1 KHz for current clamp recordings. The plotted current traces were low pass filtered again at 20 Hz.

Current injection experiments were conducted under current clamp mode in whole cell configuration with the following step protocol. First five sweeps were applied with 1 pA increment from 0 to 4 pA, followed by a second five–sweeps with 3 pA increment from 5 to 17 pA and a third five–sweeps with 5 pA increment from 15 to 35 pA. Change in spike frequency was calculated by subtracting resting frequency during current injection.

Unless otherwise indicated, the pipettes were filled with intracellular solution containing (in mM): KCl 130, $MgCl_2$ 2, KOH 10, EGTA 1, HEPES 10, ATP 5, and GTP 0.3 in pH 7.2. For internal Cl^- substitution experiments, KCl was substituted with potassium methanesulfonate (KMSF or KCH_3SO_3). For Cs^+ internal solutions, KCl was replaced with CsCl at equal molar concentration. Fluorescein–conjugated dextran (10,000) at 50mM was sometimes included in the intracellular solution to label the recorded neurons. Holding potential was −60 mV. Urine was delivered for 15 seconds using a pressurized perfusion system (ALA–VM8, ALA Scientific Instruments). The tip of the perfusion head was placed approximately 500 μm away from the slice. The time course of the perfusion was measured using a solution that contained fluorescein. It took ~300 ms from the start of the delivery for the dye signal to reach plateau value. The 15 second delivery time mimicked the duration of a typical urogenital investigation episode for the mouse. For inhibitor experiments, VNO slice was incubated in mACSF containing 100 nM apamin, 100 nM tertiapin–Q, or 100 μm SCH23390 (Sigma–Aldrich) for one minute before urine stimulus was delivered.

Excised patch single channel recording—Patches were isolated from the dendritic knob region of VNO slices. HEKA EPC 10 patch–clamp amplifier (Instrutech, Port Washington, NY) and PULSE software were used for data acquisition with Clampfit 10 (Molecular Devices, Sunnyvale, CA) for data analysis. 500 Hz 8–pole Butterworth filter was applied. Borosilicate recording pipettes were fabricated by P–2000 micropipette puller (Sutter Instrument) for 30–45 MΩ pipette resistance. Pipette solution contained (mM): 110 KMSF , 10 KCl, 1 MgCl2, 10 HEPES, 1 EGTA. Bath solution was used as the same pipette solution or K^+ was substituted by Na^+ if needed. The amount of calcium in bath solution was estimated using Ca–EGTA calculator (http://www.stanford.edu/~cpatton/CaEGTA–TS.htm).

EVG recordings—EVG was recorded from the microvillous surface of intact VNO sensory epithelia. The recording pipette (1–3 MΩ) was filled with solution B connected by an Ag/AgCl wire to a differential amplifier (DP–301, Warner Instruments). Solution B is consisted of (in mM): 145 NaCl, 5 KCl, 10 HEPES, 1 $MgCl_2$, 1 $CaCl_2$, adjusted to pH 7.3 and 300 mOsm. A second Ag/AgCl wire was connected to an agar bridge served as an indifferent electrode. The output signal was digitized and low pass–filtered (8–pole Bessel; corner frequency 60 Hz).

Measurement of lumenal K^+ concentration—To construct a K^+ selective electrode, the patch clamp pipette (~1 MΩ) was filled to 0.5 mm with a K^+ selective ion exchanger (World Precision Instruments), followed by the reference solution (500 mM KCl). A silver wire coated with AgCl was then immersed in the electrode solution and attached to AxonClamp 2A in order to measure the junction potential between the tip of the electrode and the sample solution. In addition, a ground electrode was connected through an $AgCl^-$ coated silver wire to the reference solution. Finally, the circuit was closed with a salt bridge connecting the sample with the reference solution. A series of standard solutions (1 mM to 500 mM KCl) was then measured to obtain the standard curve. In a dissected mouse head, the vomer bone was carefully removed to expose the VNO. The blood vessel that was covering the neuroepthilium was carefully removed to expose the underlying lumen of the VNO. Extra care was taken to ensure that no blood was contaminating the luminal surface. The exposed region was maintained under a stream of air saturated with water vapor to prevent drying of the tissue. It was then connected to the reference solution using a salt bridge. The K^+ concentration was then calculated with the measured junction potential using the Nernst Equation:

$$\Delta V = RT/nF \ln([K]ref/[K]_s)$$

where ΔV is the junction potential, $[K]_{ref}$ and $[K]_s$ are K^+ concentrations of the reference solution and the sample, respectively. As control, the surface of the temporal lobe of the cortex was measured using the same method.

Reconstitution of the lumen K^+ environment—In order to maintain high K^+ concentration environment in the lumen of VNO slice, a local perfusion system was constructed by double barreled electrode forming solution loop as illustrated in Fig. 7a. This flow of solution confined volume smaller than 30 nl and the shape was imaged during a recording session with the fluorescein contained in the high K^+ solution. With this system, we could confine the high K^+ solution to the dentritic region of VNO slice without affecting the soma. The local perfusion system is connected with an ALA–VM8 to allow quick switch between solutions containing different K^+ solutions, with or without urine.

Behavioral Assays

$SK3^{T/T}$ mice were in the C57/BL6 background. *$SK3^{-/-}$* and TRPC2/SK3 double mutant animals were fed with 200 mg/kg doxycycline diet (BioServ) and continued after weaning. Mothers of control *$SK3^{T/T}$* animals, the *$SK3^{T/T}$* and *$TRPC2^{-/-}$* mice were fed standard Lab Diet® rodent food (Picolab). *$GIRK1^{-/-}$* were inbred with each other. Both control and

experimental animals were weaned at 21 days of age, and separated into single–sex groups. Male mice were individually housed for 4–5 weeks prior to mating and aggression assays. All behavioral testing began 1 hour after commencement of the dark cycle, and was completed within 3 hours. Testing sessions were recorded using Sony TRV–88 cameras under infrared illumination and were analyzed after completion of the experiment by experienced observers blind to genotype.

Mating assay—48 hours prior to mating assays, 4–5 week old B6D2F1/J or C57Bl/6 females (Jackson laboratories) were given an injection of pregnant mare serum gonadotropin (PMSG) at 5 I.U. On the day of testing, a female mouse was introduced into the test male mouse's cage and the latency, frequency and duration of mounts, intromissions and ejaculations were scored for a 30–min period.

Aggression assay—Experimental and control male mice were tested for aggression using the resident–intruder aggression assay paradigm. The 15–min assays began when a group–housed, sexually inexperienced adult male mouse (the "intruder") of the CBA strain was introduced into an individually–housed "resident's" cage. Parameters of aggressive behavior including latency to first attack, total attack duration, and number of bites were scored, in addition to latency to first mount, the number of mounts and mount duration.

RESULTS

Urine evokes K^+ current in VNO neurons

We performed whole–cell patch clamp to record urine–evoked responses using slice preparations. In agreement with previous Ca^{2+} imaging experiments [25, 26], approximately 30% of the cells recorded with whole cell patch clamp showed reliable responses to repeated urine stimulation (66 out of 224 cells, 29.5%; Fig. 1a and b). The currents recorded from the soma were smaller than those recorded from dissociated cells [23]. The difference might reflect the attenuation by the dendritic cable properties. Nevertheless, the picoampere currents recorded in VNO slices were physiologically relevant because they were in a range that optimally triggered spiking activities of the VNO neurons (Supplementary Fig. 1a and b; also see reference 24). Because of the relatively small size of currents, we applied a threshold of 2X baseline noise after filtering to determine whether a cell had responded to urine stimulation. Responses smaller than 0.4 pA were excluded by this criterion.

Urine application induced currents ranging from −9 pA (inward current) to +3 pA (outward current) when the cells were voltage clamped at −60 mV (Fig. 1b). Similarly diverse response profiles were also observed under current clamp. The diverse range of responses likely reflected the heterogeneous population of VNO neurons expressing different VRs and the complex composition of urine. Among the responding cells, approximately 6% of the VNO neurons showed outward currents upon urine application (Fig. 1b). In current clamp recordings, cells responded to urine stimulation with depolarization as well as hyperpolarization (Supplementary Fig. 1c and d). Cells that exhibited a hyperpolarizing response remained hyperpolarized for a duration that was significantly longer than urine application (Supplementary Fig. 1d). The cellular mechanism of the prolonged hyperpolarization was unknown.

To assess the contribution of K^+ channels to urine–evoked responses, we first substituted the intracellular K^+ with the impermeable Cs^+. At −60 mV, current recorded with CsCl internal solution was ~54% larger than those with KCl internal solutions, suggesting that an efflux of K^+ ions counteracted and reduced the inward current (Fig. 1a).

In recent studies, we and others have shown the involvement of CACCs in mediating inward currents [23, 24]. In order to investigate the relationship among currents mediated by TRPC2, CACCs and the K^+ channels, we substituted intracellular Cl^- with non–permeable methanesulfonate (MSF^-) to eliminate the contribution of Cl^- conductance to urine–induced currents. In wildtype cells, the current was reduced by ~50% when recorded with MSF^- intracellular solutions (Fig. 1c). In *TRPC2*$^{-/-}$ VNO neurons, average current recorded using KCl^-based intracellular solution was reduced by ~35% compared to wildtype cells (Fig. 1c). The differences in current amplitude reflected the contribution of TRPC2 and CACC to VNO activation.

In *TRPC2*$^{-/-}$ neurons, TRPC2 and CACCs were not expected to contribute to urine–evoked currents when KMSF intracellular solution was used. Under this condition, strikingly, we observed an outward current in response to urine application (1.60 ± 0.24 pA; Fig. 1c). This outward current was completely abolished when intracellular K^+ was replaced with impermeable Cs^+ ions, suggesting that the outward current was a K^+ conductance (Fig. 1c). These results indicated that in the wildtype neurons, the TRPC2 channel and the Cl^- conductance carried inward current, whereas K^+ currents flowed in the opposite direction reducing the overall current size. These results further suggested that the activation of the Cl^- and K^+ conductance was not entirely dependent on TRPC2 activation. Eliminating the contribution of Cl^- conductance in *TRPC2*$^{-/-}$ neurons revealed the outward K^+ conductance.

SK3 participates in urine–evoked responses

Our data suggested that K^+ channels played a role in mediating urine–triggered responses in VNO. By RT–PCR analyses, we were able to detect the expression of SK3 and GIRK1 in the VNO, consistent with a recent report on the expression of various K^+ channels in the VNO[25]. *In situ* hybridization showed strong signals for *sk3* but far weaker signals for *sk1* and *sk2* transcripts (Fig. 2a). Immunofluorescent staining for SK3 showed high levels of SK3 expression in the cell bodies and the dendritic knobs (Fig. 2b) that co–localized with the TRPC2 (Fig. 2c). Unlike the TRPC2 staining, however, we also observed strong SK3 signals along the dendritic shank of the neurons.

We next examined whether the SK3 current was involved in VNO activation. Application of apamin, a potent blocker of SK channels, resulted in a ~2X increase of urine–evoked whole cell inward currents, consistent with our observation that K^+ carried outward currents (Fig. 2d and Supplementary Fig. 2a). In current clamp recordings, we observed an increased firing rate in response to urine application in the presence of apamin (Fig. 3c and d). In the subset of cells in which urine application induced hyperpolarization and a decrease in firing rate, apamin application led to depolarization and an increase in firing rate (Supplementary Fig. 2d). Additionally, only after urine application did we observe a marked slow after–hyperpolarization potential (sAHP) following a spike train induced by current injection and

it was blocked by apamin (Supplementary Fig. 2b and c). The apamin–sensitive sAHP was a hallmark of the activation of SK type of K^+ channels.

Our previous study demonstrated that, in the absence of TRPC2, Ca^{2+} release from intracellular stores could activate CACC currents [24]. We investigated the IP3–mediated Ca^{2+} mobilization in activating the K^+ current by using ruthenium red [11, 26]. Ruthenium red inhibited the urine–evoked outward current in *TRPC2*$^{-/-}$ neurons recorded with KMSF intracellular solution (Fig. 2e). The ruthenium red sensitive outward current was also inhibited by apamin (Fig. 2e). Although other channels might be sensitive to ruthenium red, our results were consistent with the notion that the activation of the SK3 current could be independent of TRPC2–mediated Ca^{2+} entry and Ca^{2+} was required for activating the K^+ channels.

GIRK channels participate in urine–evoked responses

In immunofluorescent staining experiments, we observed GIRK1 expression in both the cell bodies and dendrites (Fig. 3a). From the morphological features of the staining, we concluded that the GIRK channels were enriched in the VNO dendrite, with a pattern similar to that of TRPC2 expression. GIRK1 expression was also found in the dendritic shanks and not restricted to the dendritic knobs.

In pharmacological experiments, we found that two GIRK specific blockers, SCH23390 and tertiapin–Q, had similar effects in enhancing urine–activated current (Fig. 3b Supplementary Fig. 3a and b). Current clamp recordings also showed an increase in firing rate in the presence of tertiapin–Q compared to urine alone treatment (Fig. 3c and e). Thus, GIRK1 participated in urine–evoked responses. In a separate experiment, we directly infused GTP–γ–s, a non–hydrolyzable G–protein activator, through the recording pipette. GTP–γ–s caused a profound hyperpolarization of the membrane potential (Supplementary Fig. 3c–e) and a significant decrease in the spontaneous firing rate (Supplementary Fig. 3f). This G protein–induced hyperpolarization was dependent on GIRK channels (see below).

Urine–evoked response in *SK3*$^{-/-}$ and *GIRK1*$^{-/-}$ VNO$_S$

We next examined urine–evoked currents in the VNO neurons from mice deficient of SK3 or GIRK1 channels. We studied urine–evoked response in a mouse line (*SK3*$^{T/T}$) in which the expression of SK3 could be inducibly silenced by doxycycline (DOX) treatment [27]. In the VNO from *SK3*$^{T/T}$ mice fed with DOX, we found no detectable SK3 expression, whereas high levels of SK3 expression were found in mice fed with regular diet (Fig. 4a). In the VNO of these *SK3*$^{-/-}$ mice, apamin application no longer increased the size of current induced by urine stimulation (Fig. 4b and Supplementary Fig. 4a). However, tertiapin–Q application was able to augment the response (Fig. 4b and Supplementary Fig. 4b).

Because GIRK1 was shown to be obligatory for the proper function of all GIRK channels [28, 29], we examined urine–evoked currents in *GIRK1*$^{-/-}$ mutant mice [30]. We confirmed the absence of GIRK1 channels in the VNO of the mutant animals with immunofluorescent staining (Fig. 4c). Analysis of urine–evoked responses of VNO neurons from *GIRK1*$^{-/-}$ mice revealed that urine–evoked current was no longer sensitive to

tertiapin–Q (Fig. 4d and Supplementary Fig. 4c) but was augmented by apamin (Fig. 4d and Supplementary Fig. 4d). Moreover, infusion of GTP–γ–s through the patch pipette did not alter the resting potential or spontaneous spiking rate of the VNO neurons from *GIRK1*$^{-/-}$ mice (Supplementary Fig. 4e–h).

Single channel activities of SK3 and GIRK channels in the VNO dendrite

We next conducted single channel recording in excised patches from the VNO neuron dendrites in the slice preparations (Fig. 5a). In inside–out patches excised from wildtype VNO, elevating the intracellular Ca^{2+} concentration elicited single channel activities (Fig. 5b). In isotonic K^+ condition, the channels had a single channel conductance of 10.08 ± 0.46 pS with no obvious rectification (Fig. 5b and c). Replacing extracellular K^+ with Na^+ shifted the reversal potential from ~0mV to ~ −50mV, near the reversal potential of K^+ (Fig. 5c). The single channel properties of this channel type were consistent with those reported for SK3[31]. In out–side–out patches with elevated intracellular Ca^{2+}, the single channel activity was blocked by a brief application of apamin (Fig. 5d).

Similarly, exposing the intracellular side of the patch to purified 5 nM $G_{\beta\gamma}$ subunits led to channel activities that were distinct from the action of Ca^{2+} (Fig. 5e). The single channel conductance under isotonic K^+ condition was 15.24 ± 0.78 pS (Fig. 5f). The shift in reversal potential by replacing extracellular K^+ with Na^+ was similar to that of the Ca^{2+} –activated channels (Fig. 5f). The single channel properties of the $G_{\beta\gamma}$–activated channels were consistent with the ones reported for the small conductance GIRK channels [32]. Applying $G_{\beta\gamma}$ together with elevated Ca^{2+} led to the opening of both type of channels in the same patch (Fig. 5g).

We performed similar experiments in the *SK3*$^{-/-}$ and *GIRK1*$^{-/-}$ mice (Fig. 5h&i). In *SK3*$^{-/-}$ mice, the 10 pS activity was absent with elevated Ca^{2+} (5 out of 5 patches) but the 15 pS channels was activated by $G_{\beta\gamma}$ (Fig. 5h). Conversely, in *GIRK1*$^{-/-}$ mice, the 10 pS channel was activated by Ca^{2+} but $G_{\beta\gamma}$ did not activate the 15 pS channels (4 out of 4 patches; Fig. 5i). The properties of these single channels were consistent with the presence of SK3 and GIRK in the VNO dendrites.

Taken together, the data obtained from the mutant mice confirmed the participation of both SK3 and GIRK channels in urine–induced response in the dendrites of the VNO neurons. Their actions were independent of each other. Moreover, the finding of both types of single channel activities in the same patch was consistent with the coexpression of SK3 and GIRK1 channels in the same neuronal population. These observations suggested that both signaling pathways were present in the same neurons.

The paradox of urine–induced K^+ current in the VNO

In order to obtain a comprehensive view of the K^+ conductance in the VNO neuronal population, we performed electrovomeronasogram (EVG), extracellular field potential recording from the VNO dendritic surface. We recorded EVG signals from a total of over 55 wildtype mice and 23 mutant animals with more than 250 recordings (3–6 recordings per animal). In wildtype mice, application of urine mixtures elicited downward voltage

deflections that were indicative of inward currents in the intact VNO (Fig. 6a). Based on our patch clamp results, we expected that applying apamin or tertiapin–Q would increase the size of EVG responses. Surprisingly, we found that blocking of the SK3, GIRK or both channels reduced the responses by 46.5%, 58.7% and 71.2 %, respectively (Fig. 6a).

We next examined the EVG responses in wildtype, *SK3*$^{-/-}$, *GIRK1*$^{-/-}$ as well as *TRPC2*$^{-/-}$ mice. Consistent with the result of pharmacological blockers, the peak EVG responses to urine were reduced by approximately 21.3%, 28.2% and 49.8% in *TRPC2*$^{-/-}$, *GIRK1*$^{-/-}$ and *SK3*$^{-/-}$ mutants, respectively (Fig. 6b). There was a 58.8% reduction in EVG responses in SK3/TRPC2 double mutants (Fig. 6b).

K^+ environment in the lumen of the VNO

It was surprising that blocking K^+ currents significantly diminished urine–evoked response in intact tissue. Neurons normally maintain high intracellular K^+. Opening of K^+ channels leads to K^+ efflux and an outward current. In intact VNO, however, urine–evoked activation of the K^+ channels appeared to contribute to an inward current. This observation also presented a paradox because data obtained from intact tissue (EVG) and from slice preparations (patch clamp) gave opposite conclusions. This apparent paradox could be explained if the dendrites of the VNO neurons were exposed to a local environment that was rich in K^+, a situation resembling that of the cochlear hair cells, where K^+ rich endolymphs led to K^+ influx through the tip–link channels to depolarize the neurons. High external K^+ in the VNO lumen would set the K^+ reversal potential at the dendrites to a positive value to result in K^+ influx through SK3 and GIRK channels. If the high K^+ environment was washed away in the slice preparations, the efflux of K^+ would generate outward currents.

We measured the K^+ concentration in the VNO lumen using a K^+–selective electrode (Fig. 7a). As control, the surface of the temporal lobe of the cortex was measured using the same method. Six independent measurements showed that K^+ concentrations in the lumen of the VNO (66 ± 36 mM) were significantly greater than those observed at the cortical surfaces (17 ± 6 mM; Fig. 7b). The reversal potential in VNO dendrites was calculated to be approximately −18 mV, well above the VNO resting potential (around −50mV). Thus K^+ channel activation at the dendrites would generate an inward K^+ conductance to depolarize the VNO neurons.

Reconstitution of the native K^+ environment

We sought to experimentally reconstitute the high K^+ environment in slice preparations. Since the maintenance of high intracellular K^+ and low extracellular K^+ was essential to sustain the electrical gradient necessary for neuronal function, the K^+ environments must be compartmentalized such that only the neuronal dendrites were exposed to high K^+ in the lumen, whereas the cell bodies were in a low K^+ environment. Recapitulation of the *in vivo* ionic environments in slice preparations therefore required the construction of compartments such that the soma and dendrites were exposed to different concentrations of K^+. This was a technical challenge because the soma and dendrites were only approximately 30–100 μm apart in a slice. We devised a local perfusion system that confined solution flow in a volume smaller than 30 nl. This allowed the selective perfusion of high K^+ solution to the dendrites

but not to the soma (Fig. 7c). The high K^+ solution, visualized by imaging of fluorescein dye, was confined to the tip of the perfusion head and could be precisely manipulated (Fig. 7d). When the local perfusion of high K^+ solution was confined to the dendritic region of the VNO slice (Fig. 7d), there was little change in firing rate of the cells (Fig. 7d). By moving the tip close to the cell body, we observed a robust increase in the spontaneous firing that saturated, presumably because of the direct depolarization of the neurons (Fig. 7e). These observations indicated that we could successfully compartmentalize the K^+ environment in the slice preparations. The dendritic K^+ channels appeared to be inactive under normal circumstances because the cells were not excited when their dendrites were exposed to high K^+ environment before urine stimulation was presented.

We examined the response of VNO neurons to urine stimulation under the reconstituted K^+ environment using cell–attached extracellular recordings. By switching the dendritic K^+ solution from low to high concentrations, we observed a general increase in urine–induced spiking rate. However, it was not clear whether the increase in spiking rate was the result of inverted K^+ flow or from an overall depolarizing effect of K^+ at the dendrites. Therefore, we sought cells that showed a decreased firing rate in response to urine stimulation (Fig. 7f). Although these cells were rare (~6% of responding cells; Fig. 1b), they provided an unambiguous demonstration of inverted flow of K^+ at the dendrites. We were able to obtain three cells in this type of recordings. In one such example (Fig. 7e–g), exposure to urine under low external K^+, in mACSF, resulted in a prolonged decrease in the firing rate of the cell, similar to what was observed in current clamp experiments (Supplementary Fig. 1d). Subsequent exposure of the dendrites to a high K^+ environment did not reverse the depressed firing rate (Fig. 7f). However, when urine was used to stimulate the dendrite in the high K^+ solution, the neuron responded with a robust increase in firing rates (Fig. 7g). We also conducted the converse experiment by first exposing the dendrites to high K^+ solution and then switching to mACSF. Urine stimulation under this configuration induced a robust increase in spiking rate that was immediately reversed when external solution at the dendrites was switched to mACSF containing diluted urine (Fig. 7h). Thus, we were able to record from individual neurons under a reconstituted lumenal environment and to demonstrate that the sign of responses were critically dependent on the K^+ concentrations at the dendrites.

Aggressive and mating behaviors in *SK3*$^{-/-}$ and *GIRK1*$^{-/-}$ mutant mice

We examined innate behaviors in *SK3*$^{-/-}$ and *GIRK1*$^{-/-}$ mice. In resident–intruder aggression assays, *SK3*$^{-/-}$ mice exhibited a significant reduction in all parameters of aggressive behaviors including latency to first attack and attack frequency when compared with controls (Fig. 8a). In mating assays, we observed that sexually naïve *SK3*$^{-/-}$ males displayed a longer latency to first mount when paired with females (Fig. 8b). Similarly, *GIRK1*$^{-/-}$ mice also displayed longer latency and lower frequency in both aggression and mating assays (Fig. 8c and d).

Thus, silencing of SK3 expression resulted in abnormalities in both mating and aggressive behaviors. This observation was consistent with the notion that K^+ current mediates VNO excitation. We noted that the extent of suppression of aggressive behavior in *SK3*$^{-/-}$ or

GIRK$^{-/-}$ mice was not so profound as reported previously for *TRPC2*$^{-/-}$ males, which did not display aggressive attacks to intruder males (Fig. 8e). On the other hand, we noted that silencing SK3 or GIRK1 had a more profound effect on the sexual behaviors of the animals than TRPC2 mutants, in which male–female sexual behavior appeared normal (Fig. 8e). We wondered whether removing a K^+ channel in addition to TRPC2 would exacerbate the behavioral phenotypes. We investigated the innate behaviors of SK3/TRPC2 double mutants. Consistent with the electrophysiological data, fewer double mutant animals than *SK3*$^{-/-}$ displayed aggression towards intruders and mounted females (Fig. 8e). We also noticed that the percentage of double mutant animals displaying male–to–male mounting was reduced compared with *TRPC2*$^{-/-}$ males. The reduction in the number of aggressive animals and the increase in males displaying male–to–male mounting appeared to be associated with *TRPC2*$^{-/-}$ genotype. There was not statistical significance between *TRPC2*$^{-/-}$ and *SK3*$^{-/-}$ / *TRPC*$^{-/-}$ mutants in these tests (Fig. 8e; Table S1).

DISCUSSION

The role of K^+ channels in VNO signaling

Several groups have reported the participation of K^+ channels in determining the electrophysiological properties of the VNO neurons. Two groups have reported that the large conductance Ca^{2+}–activated K^+ channel (BK) is responsible for outward current in VNO neuron [33, 34], which appears to set the rhythmic firing of the VNO neurons. Another study has found activity–dependent expression of ERG K^+ channel, which appears to control sensory output in VNO neurons [25]. Our study, on the other hand, uncovers a role of K^+ channels in mediating the primary response of the VNO neurons. The action of currents mediated by GIRK and SK3 resembles the signaling mechanism of the cochlear hair cells in the acoustic organ of Corti, where high K^+ in the endolymph leads to the influx of K^+ ions to depolarize the cells.

Model of VNO signal transduction

Based on our results and other published studies, we propose a revised model of VNO activation. In this model, ligand recognition by a vomeronasal receptor initiates two separate intracellular pathways. The release of $G_{\beta\gamma}$ subunits directly activates the GIRK channels. On the other hand, increased activity of PLC produces elevated levels of IP3 and DAG. DAG is likely to directly activate the TRPC2 channel [16], whereas IP3 can mobilize intracellular Ca^{2+} stores through the IP3 receptors [11, 35]. The increase in intracellular Ca^{2+} concentration from the stores appears sufficient to activate the SK3 and the CACCs to depolarize the cell. The influx of cations through the TRPC2 channel not only depolarizes the cell, but also contributes to the increase of intracellular Ca^{2+} to augment SK3 and CACC activation. We note that Ca^{2+}–sensitive cation channels and an arachidonic acid–sensitive current have also been found in the VNOs [13, 21, 22, 36]. It is possible that yet more channels participate in VNO signaling.

Our results address a puzzle in VNO signaling. The mammalian VNO expresses two main G–proteins, G_{i2} and G_o. Both are considered “inhibitory” as their roles have been shown to inhibit cyclase activities. The release of βγ subunits from the G_{i2} and G_o complex have also

been shown to activate GIRK channels to cause hyperpolarization of cells. It has been enigmatic how inhibitory G–proteins contribute to VNO excitation. Our results demonstrate that the GIRK channels indeed contribute to the activation of the VNO neurons. Together with the SK3 channels, they contribute to a paradoxical influx of K^+ ions that enhances the pheromone–induced depolarization.

Our observations explain the difficulties in recording from VNO slices. In VNO slices, the efflux of K^+ counteracts the inward currents mediated by TRPC2 and CACCs, leading to a reduction of the overall current size. Because the current needed to depolarize VNO neurons is small, the counter flow of K^+ ions makes it even harder to detect currents evoked by urine stimulation. We note that the size of current recorded in slice preparations is smaller than that from the dissociated cells. This could be explained by the intact dendritic morphology maintained in slice preparations — the amplitude of the urine–evoked current at the dendritic knob may be attenuated by the cable properties of the dendrites. The larger currents observed in dissociated cells may also be attributed to a loss of the dendritically located K^+ channels to allow larger currents to be detected.

Our observations may also reconcile the inconsistencies in VNO response to external stimulations reported by different groups. The discrepancies could be explained by experimental conditions that favored one type of current or another. In one study of dissociated neurons, Moss and colleagues have reported that urine induced an outward current from mouse VNO neurons, whereas Fadool and colleagues have reported urine–evoked currents of either polarities in different VNO neurons in turtle and lizard [37–40]. These studies used KCl as the main ions in intracellular solutions, thus allowing the contribution of both K^+ and Cl^-. In contrast, studies that used CsCl as internal solutions reported mostly inward currents [16, 23, 24, 33]. In intact tissue preparations, only an increase in the firing rate from the VNO neurons was reported, possibly as the result of retention of the intact K^+ environment [41].

Independent pathways for VNO activation

TRPC2 channel has been considered as the main contributor to VNO signaling. Our model places the K^+ channels and the CACCs into pheromone signaling pathways parallel to TRPC2. The currents mediated by SK3 and GIRK appear to be part of a primary response induced by urine independent on TRPC2 or CACCs; the K^+ currents are activated in the absence of TRPC2 and CACC currents.

The existence of parallel pathways in VNO is in direct contrast of signal transduction in the MOE [42]. In the MOE, the activation of the CACC is secondary to the CNG channels. In the VNO, TRPC2 is not indispensible for the activation of either SK3 or CACC, but it can facilitate the activation of these channels by allowing Ca^{2+} influx into the neuron. Ca^{2+} entry through TRPC2 can act synergistically with Ca^{2+} release from intracellular stores to activate SK3 and CACC. These observations are consistent with previous studies suggesting TRPC2–independent activation of the VNO [13, 36].

Innate behaviors of *SK3*$^{-/-}$, *GIRK1*$^{-/-}$ and *TRPC2*$^{-/-}$ mice

Deficits in mating and aggression behaviors are observed in *SK3*$^{-/-}$ mice and *GIRK1*$^{-/-}$ mice, further supporting an important role of the K^+ channels in VNO function. However, there are important discrepancies in mating and aggressive behaviors between *SK3*$^{-/-}$, *GIRK1*$^{-/-}$ and *TRPC2*$^{-/-}$ mice. Mating with females is affected in *SK3*$^{-/-}$ and *GIRK1*$^{-/-}$, but not in *TRPC2*$^{-/-}$ mice. On the other hand, the extent of the suppression of aggression in *SK3*$^{-/-}$ or *GIRK1*$^{-/-}$ mice is not as profound as observed in TRPC2 mutant males [18–20]. It is important to note that the knockout of the SK3 and GIRK1 channel is not restricted to the VNO, nor is TRPC2. Silencing of these genes in brain regions other than the VNO may contribute to the observed deficits in mating and aggression. Alternatively, it is possible that distinct populations of neurons reside within the VNO and the relative contribution of TPRC2, SK3 and GIRK1 differs in different cells.

Noticeably male–male mounting is observed with far greater frequency in TRPC2 mutants than in wild type mice and is not observed in *SK3*$^{-/-}$, *GIRK1*$^{-/-}$ mice or in mice with VNO surgically removed. The frequency is also reduced in TRPC2/SK3 double mutants. It is also worth noting that in mice missing G_{i2} or G_o proteins, no male–to–male mounting behaviors were observed [43, 44]. Thus, the male–male mounting is likely specific to *TRPC2*$^{-/-}$ mice. A plausible explanation of this phenotype in the *TRPC2*$^{-/-}$ mice is the selective loss of the basal layer of VNO neurons. In *TRPC2*$^{-/-}$, more than 50% of the basal layer of neurons, which express the V2R family of vomeronasal receptors and the G_o protein, are lost (Fig. S5) [18]. The apical layer, which expresses the V1Rs, appears relatively intact. *TRPC2*$^{-/-}$ mice also display differential hypotrophy of the glomerular layer of the AOB, with the anterior portion (the G_{i2} zone) intact but the posterior portion (G_o zone) reduced or absent [45]. Consistent with these results, recording from the basal layer of neurons using multielectrode showed a dramatic decrease in urine–evoked responses [18], whereas sampling of the whole population with EVG recordings, or recording from dissociated cells, revealed residual responses [19, 36, 46]. It is therefore possible that the contribution by the V2R expressing neurons is more severely affected than the apical cells in *TRPC2*$^{-/-}$ mice. The differential effects on the two anatomically segregated neuronal populations may create an imbalance of pheromone signaling to the brain. This imbalance, together with reduced activation of the remaining cells, may lead to the male–male mounting phenotypes observed in the *TRPC2*$^{-/-}$ mice. *SK3*$^{-/-}$ and *GIRK1*$^{-/-}$ mice does not appear to have the selective loss of neurons.

Sensitivity and robustness of urine–evoked responses

The VNO is highly sensitive to pheromones [47, 48]. This sensitivity is the result of specific interaction between the ligand and the receptor, the amplification of signals transduced by receptor occupancy, and the sensitivity in generating membrane currents. VNO neurons maintain depolarized membrane potentials at rest along with high input resistance [11, 38, 49]. As we and others have shown, the neurons are exquisitely sensitive to small currents [24, 49]. The depolarized resting potential allows the neurons to rest close to the detection threshold while the high input resistance allows excitation by small electrical input, which significantly enhances the sensitivity of VNO neurons in response to pheromone stimuli.

The high level of sensitivity to small currents may allow the contributions of several ion species to activate the VNO and enables the VNO to accommodate to different external ionic environments. Pheromones are contained in saliva, body and gland secretions, as well as fecal and urinary excretions. These sources are high in salt content. The VNO, therefore, must be able to cope with the variation of salt concentrations. By permitting most common ions (Na^+, K^+ and Cl^-) to contribute to the depolarization of the neurons, the VNO response is less influenced by changes in the environment. Hence, the VNO is one of several sensory systems that have evolved specialized transduction mechanisms that exploit unique ionic environments to enhance signal transduction and to accommodate their distinct functional requirements.

Supplementary Material

Refer to Web version on PubMed Central for supplementary material.

ACKNOWLEDGEMENTS

We are truly grateful for the continuing support and guidance from Dr. Richard Axel, from whose laboratory this work was originated. We appreciate the generosity of Dr. Kevin Wickman for providing the *GIRK1*$^{-/-}$ mice and Dr. Emily Liman for providing the TRPC2 antibodies. We thank Andrea Moran, Sara Klinefelter and the Lab Animal Services at the Stowers Institute for technical assistance. We thank Dr. Sachiko Haga–Yamanaka for critical comments on the paper, Drs. Hua Li and Lakshmi Chandrasekaran for statistical consultation and Colleen McLaughlin for editorial assistance. This work is supported by funding from the Stowers Institute and the NIH (NIDCD 008003) to CRY. The content is solely the responsibility of the authors and does not necessarily represent the official views of the National Institute on Deafness and Other Communication Disorders or the National Institutes of Health.

References

1. Halpern M. The organization and function of the vomeronasal system. Annu Rev Neurosci. 1987; 10:325–362. [PubMed: 3032065]
2. Tirindelli R, Dibattista M, Pifferi S, Menini A. From pheromones to behavior. Physiol Rev. 2009; 89:921–956. [PubMed: 19584317]
3. Meredith M. Chronic recording of vomeronasal pump activation in awake behaving hamsters. Physiol Behav. 1994; 56:345–354. [PubMed: 7938248]
4. Dulac C, Axel R. A novel family of genes encoding putative pheromone receptors in mammals. Cell. 1995; 83:195–206. [PubMed: 7585937]
5. Herrada G, Dulac C. A novel family of putative pheromone receptors in mammals with a topographically organized and sexually dimorphic distribution. Cell. 1997; 90:763–773. [PubMed: 9288755]
6. Matsunami H, Buck LB. A multigene family encoding a diverse array of putative pheromone receptors in mammals. Cell. 1997; 90:775–784. [PubMed: 9288756]
7. Pantages E, Dulac C. A novel family of candidate pheromone receptors in mammals. Neuron. 2000; 28:835–845. [PubMed: 11163270]
8. Ryba NJ, Tirindelli R. A new multigene family of putative pheromone receptors. Neuron. 1997; 19:371–379. [PubMed: 9292726]
9. Riviere S, Challet L, Fluegge D, Spehr M, Rodriguez I. Formyl peptide receptor-like proteins are a novel family of vomeronasal chemosensors. Nature. 2009; 459:574–577. [PubMed: 19387439]
10. Liberles SD, et al. Formyl peptide receptors are candidate chemosensory receptors in the vomeronasal organ. Proc Natl Acad Sci U S A. 2009; 106:9842–9847. [PubMed: 19497865]
11. Inamura K, Kashiwayanagi M, Kurihara K. Inositol-1,4,5-trisphosphate induces responses in receptor neurons in rat vomeronasal sensory slices. Chem Senses. 1997; 22:93–103. [PubMed: 9056089]

12. Sasaki K, Okamoto K, Inamura K, Tokumitsu Y, Kashiwayanagi M. Inositol-1,4,5-trisphosphate accumulation induced by urinary pheromones in female rat vomeronasal epithelium. Brain Res. 1999; 823:161–168. [PubMed: 10095022]
13. Spehr M, Hatt H, Wetzel CH. Arachidonic acid plays a role in rat vomeronasal signal transduction. J Neurosci. 2002; 22:8429–8437. [PubMed: 12351717]
14. Kroner C, Breer H, Singer AG, O'Connell RJ. Pheromone-induced second messenger signaling in the hamster vomeronasal organ. Neuroreport. 1996; 7:2989–2992. [PubMed: 9116225]
15. Liman ER, Corey DP, Dulac C. TRP2: a candidate transduction channel for mammalian pheromone sensory signaling. Proc Natl Acad Sci U S A. 1999; 96:5791–5796. [PubMed: 10318963]
16. Lucas P, Ukhanov K, Leinders-Zufall T, Zufall F. A diacylglycerol-gated cation channel in vomeronasal neuron dendrites is impaired in TRPC2 mutant mice: mechanism of pheromone transduction. Neuron. 2003; 40:551–561. [PubMed: 14642279]
17. Vannier B, et al. Mouse trp2, the homologue of the human trpc2 pseudogene, encodes mTrp2, a store depletion-activated capacitative Ca2+ entry channel. Proc Natl Acad Sci U S A. 1999; 96:2060–2064. [PubMed: 10051594]
18. Stowers L, Holy TE, Meister M, Dulac C, Koentges G. Loss of sex discrimination and male-male aggression in mice deficient for TRP2. Science. 2002; 295:1493–1500. [PubMed: 11823606]
19. Leypold BG, et al. Altered sexual and social behaviors in trp2 mutant mice. Proc Natl Acad Sci U S A. 2002; 99:6376–6381. [PubMed: 11972034]
20. Kimchi T, Xu J, Dulac C. A functional circuit underlying male sexual behaviour in the female mouse brain. Nature. 2007; 448:1009–1014. [PubMed: 17676034]
21. Liman ER. Regulation by voltage and adenine nucleotides of a Ca2+-activated cation channel from hamster vomeronasal sensory neurons. J Physiol. 2003; 548:777–787. [PubMed: 12640014]
22. Spehr J, et al. Ca2+ -calmodulin feedback mediates sensory adaptation and inhibits pheromone-sensitive ion channels in the vomeronasal organ. J Neurosci. 2009; 29:2125–2135. [PubMed: 19228965]
23. Yang C, Delay RJ. Calcium-activated chloride current amplifies the response to urine in mouse vomeronasal sensory neurons. J Gen Physiol. 2010; 135:3–13. [PubMed: 20038523]
24. Kim S, Ma L, Yu CR. Requirement of calcium-activated chloride channels in the activation of mouse vomeronasal neurons. Nat Commun. 2011; 2:365. [PubMed: 21694713]
25. Hagendorf S, Fluegge D, Engelhardt C, Spehr M. Homeostatic control of sensory output in basal vomeronasal neurons: activity-dependent expression of ether-a-go-go-related gene potassium channels. J Neurosci. 2009; 29:206–221. [PubMed: 19129398]
26. Inamura K, Kashiwayanagi M, Kurihara K. Blockage of urinary responses by inhibitors for IP3-mediated pathway in rat vomeronasal sensory neurons. Neurosci Lett. 1997; 233:129–132. [PubMed: 9350849]
27. Bond CT, et al. Respiration and parturition affected by conditional overexpression of the Ca2+-activated K+ channel subunit, SK3. Science. 2000; 289:1942–1946. [PubMed: 10988076]
28. Krapivinsky G, et al. The G-protein-gated atrial K+ channel IKACh is a heteromultimer of two inwardly rectifying K(+)-channel proteins. Nature. 1995; 374:135–141. [PubMed: 7877685]
29. Hedin KE, Lim NF, Clapham DE. Cloning of a Xenopus laevis inwardly rectifying K+ channel subunit that permits GIRK1 expression of IKACh currents in oocytes. Neuron. 1996; 16:423–429. [PubMed: 8789957]
30. Bettahi I, Marker CL, Roman MI, Wickman K. Contribution of the Kir3.1 subunit to the muscarinic-gated atrial potassium channel IKACh. J Biol Chem. 2002; 277:48282–48288. [PubMed: 12374786]
31. Barfod ET, Moore AL, Lidofsky SD. Cloning and functional expression of a liver isoform of the small conductance Ca2+-activated K+ channel SK3. Am J Physiol Cell Physiol. 2001; 280:C836–C842. [PubMed: 11245600]
32. Nikolov EN, Ivanova-Nikolova TT. Functional characterization of a small conductance GIRK channel in rat atrial cells. Biophys J. 2004; 87:3122–3136. [PubMed: 15507689]
33. Zhang P, Yang C, Delay RJ. Urine stimulation activates BK channels in mouse vomeronasal neurons. J Neurophysiol. 2008; 100:1824–1834. [PubMed: 18701755]

34. Ukhanov K, Leinders-Zufall T, Zufall F. Patch-clamp analysis of gene-targeted vomeronasal neurons expressing a defined V1r or V2r receptor: ionic mechanisms underlying persistent firing. J Neurophysiol. 2007; 98:2357–2369. [PubMed: 17715188]
35. Wekesa KS, Anholt RR. Pheromone regulated production of inositol-(1,4,5)-trisphosphate in the mammalian vomeronasal organ. Endocrinology. 1997; 138:3497–3504. [PubMed: 9231804]
36. Zhang P, Yang C, Delay RJ. Odors activate dual pathways, a TRPC2 and a AA-dependent pathway, in mouse vomeronasal neurons. Am J Physiol Cell Physiol. 2010; 298:C1253–C1264. [PubMed: 20147653]
37. Labra A, Brann JH, Fadool DA. Heterogeneity of voltage- and chemosignal-activated response profiles in vomeronasal sensory neurons. J Neurophysiol. 2005; 94:2535–2548. [PubMed: 15972830]
38. Fadool DA, Wachowiak M, Brann JH. Patch-clamp analysis of voltage-activated and chemically activated currents in the vomeronasal organ of Sternotherus odoratus (stinkpot/musk turtle). J Exp Biol. 2001; 204:4199–4212. [PubMed: 11815645]
39. Moss RL, et al. Urine-derived compound evokes membrane responses in mouse vomeronasal receptor neurons. J Neurophysiol. 1997; 77:2856–2862. [PubMed: 9163402]
40. Moss RL, et al. Electrophysiological and biochemical responses of mouse vomeronasal receptor cells to urine-derived compounds: possible mechanism of action. Chem Senses. 1998; 23:483–489. [PubMed: 9759537]
41. Holy TE, Dulac C, Meister M. Responses of vomeronasal neurons to natural stimuli. Science. 2000; 289:1569–1572. [PubMed: 10968796]
42. Imai T, Sakano H. Odorant receptor-mediated signaling in the mouse. Curr Opin Neurobiol. 2008; 18:251–260. [PubMed: 18721880]
43. Norlin EM, Gussing F, Berghard A. Vomeronasal phenotype and behavioral alterations in G alpha i2 mutant mice. Curr Biol. 2003; 13:1214–1219. [PubMed: 12867032]
44. Chamero P, et al. G protein G(alpha)o is essential for vomeronasal function and aggressive behavior in mice. Proc Natl Acad Sci U S A. 2011; 108:12898–12903. [PubMed: 21768373]
45. Hasen NS, Gammie SC. Trpc2 gene impacts on maternal aggression, accessory olfactory bulb anatomy and brain activity. Genes Brain Behav. 2009; 8:639–649. [PubMed: 19799641]
46. Kelliher KR, Spehr M, Li XH, Zufall F, Leinders-Zufall T. Pheromonal recognition memory induced by TRPC2-independent vomeronasal sensing. The European journal of neuroscience. 2006; 23:3385–3390. [PubMed: 16820028]
47. He J, et al. Distinct signals conveyed by pheromone concentrations to the mouse vomeronasal organ. J Neurosci. 2010; 30:7473–7483. [PubMed: 20519522]
48. Leinders-Zufall T, et al. Ultrasensitive pheromone detection by mammalian vomeronasal neurons. Nature. 2000; 405:792–796. [PubMed: 10866200]
49. Liman ER, Corey DP. Electrophysiological characterization of chemosensory neurons from the mouse vomeronasal organ. J Neurosci. 1996; 16:4625–4637. [PubMed: 8764651]

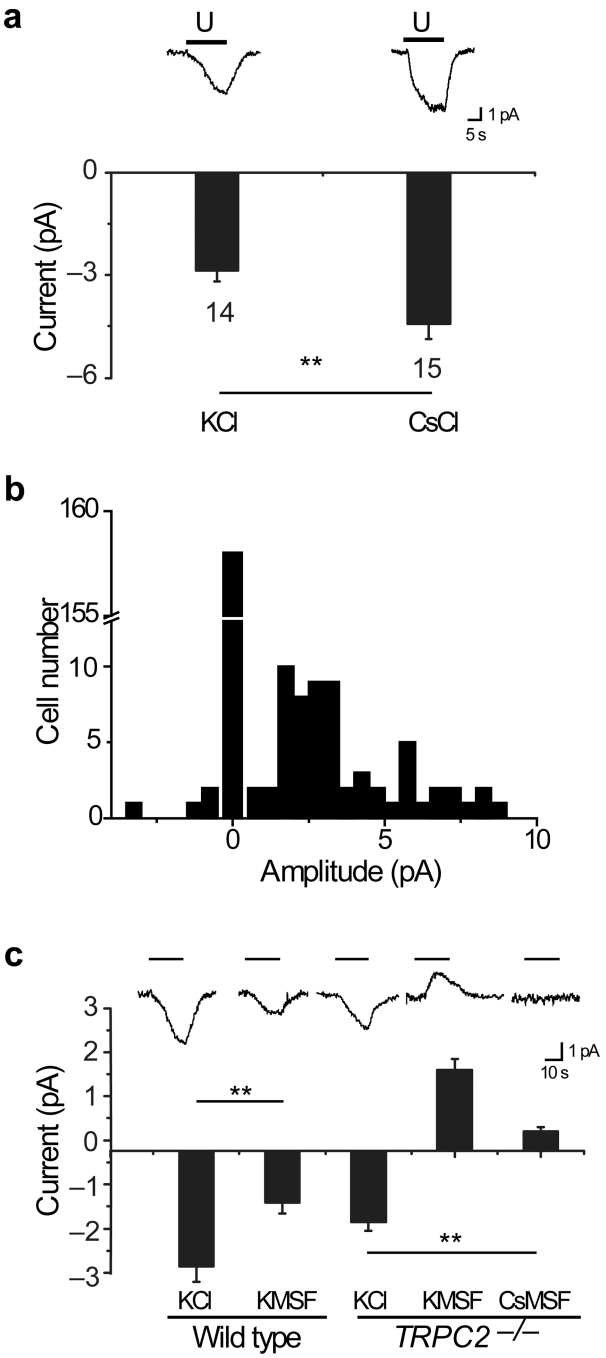

Fig. 1. Contribution of K^+ current to urine–induced responses in VNO neurons

(a) Sample traces and average urine–evoked whole cell current in VNO neurons recorded with KCl and CsCl intracellular solutions. Average whole cell response amplitudes are 2.87 ± 0.33 pA for KCl (n=14 cells) and 4.43 ± 0.44 pA for CsCl (n=15 cells). **(b)** Response amplitude distribution of the recorded cells. **(c)** Sample traces and average urine–evoked whole cell current recorded with different intracellular solutions in wildtype and *TRPC2*$^{-/-}$ neurons. Whole cell response amplitudes for KCl (same as **a**) and KMSF internal solutions in wildtype VNO neurons are 2.87± 0.33 pA (n=14 cells) and 1.43± 0.24 pA (n=8 cells),

respectively. Response amplitudes for KCl, KMSF and CsMSF in *TRPC2*$^{-/-}$ VNO are 1.86 ± 0.17 pA,−1.62 ± 0.24 pA, and −0.19 ± 0.11 pA, respectively (n=9 cells for all). Negative values of current indicate outward current. Bars above the traces indicate the duration of urine application. ** indicates p <0.01 in Student's t–test. Data are shown as mean ± SEM.

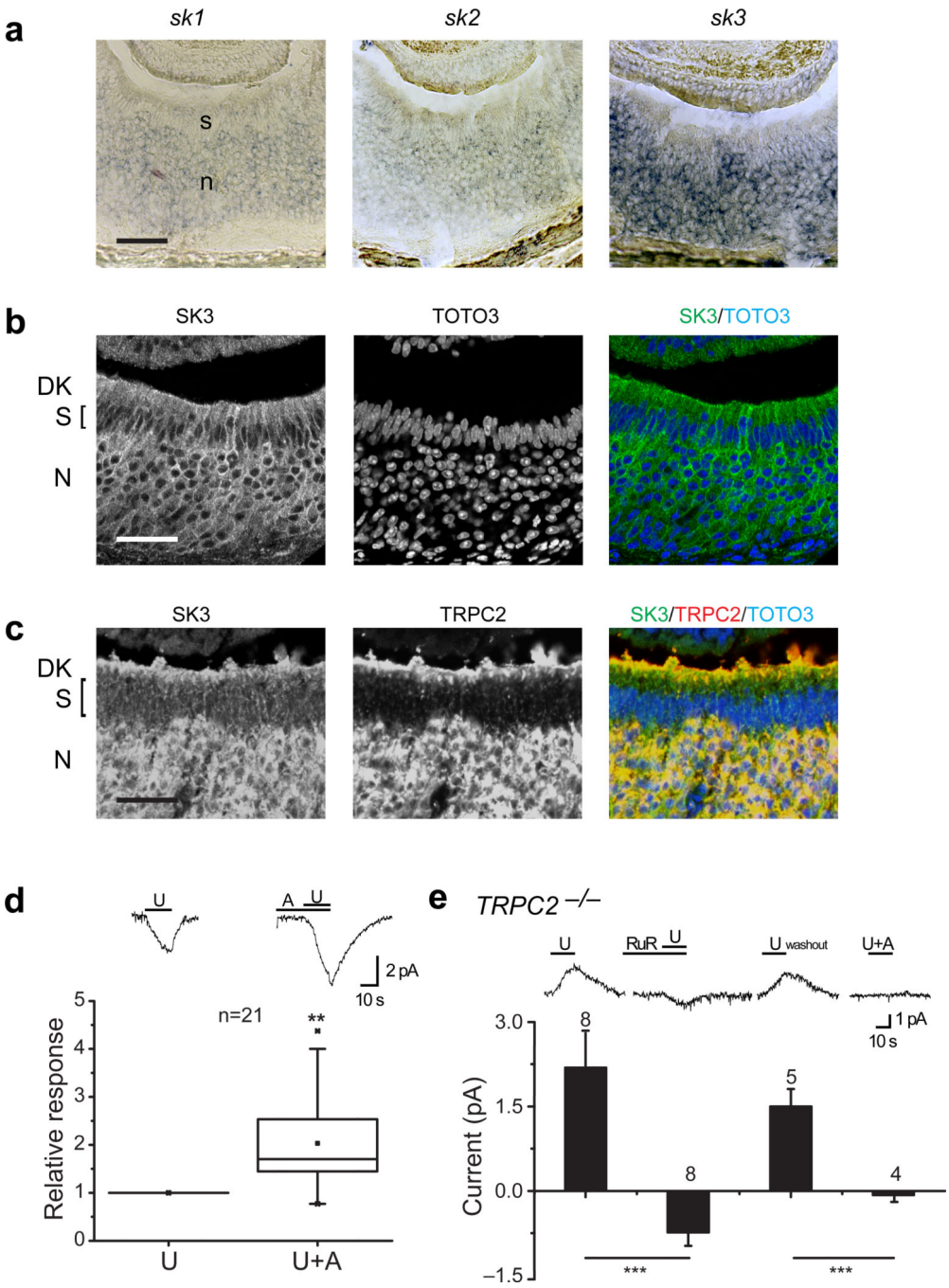

Fig. 2. Contribution of SK3 channel to VNO activation

(a) *In situ* hybridization with antisense probes specific to the *sk1*, *sk2* or *sk3* RNA. **(b)** Immunofluorescent images of VNO sections stained with antibodies recognizing SK3 (left), nuclear dye TOTO–3 (middle) and pseudocolor merged picture (right). **(c)** Immunofluorescent images of VNO sections stained with antibodies against SK3 (left), TRPC2 (middle) and pseudocolor merged picture with TOTO–3 staining (right). Scale bars in (a) – (c):50μm. **(d)** Sample traces and relative whole cell response to treatments with urine (U) or urine with apamin (A). Box plot indicates the relative changes after apamin

treatment (2.03 ± 0.97; n=21 cells). Bar graph for current amplitude is presented in Supplementary Fig. 2a. **(e)** Sample traces and average whole cell response to treatment with urine, urine after Ruthenium Red (RuR) and urine with apamin in *TRPC2*$^{-/-}$ VNO neurons. The number of cells recorded under each condition is indicated. ** indicates p <0.01 and *** indicates p <0.001 in Student's t–test. All results are expressed as the mean ± SEM. DK: dendritic knob; S: sustentacular cell layer; N: neuronal layer.

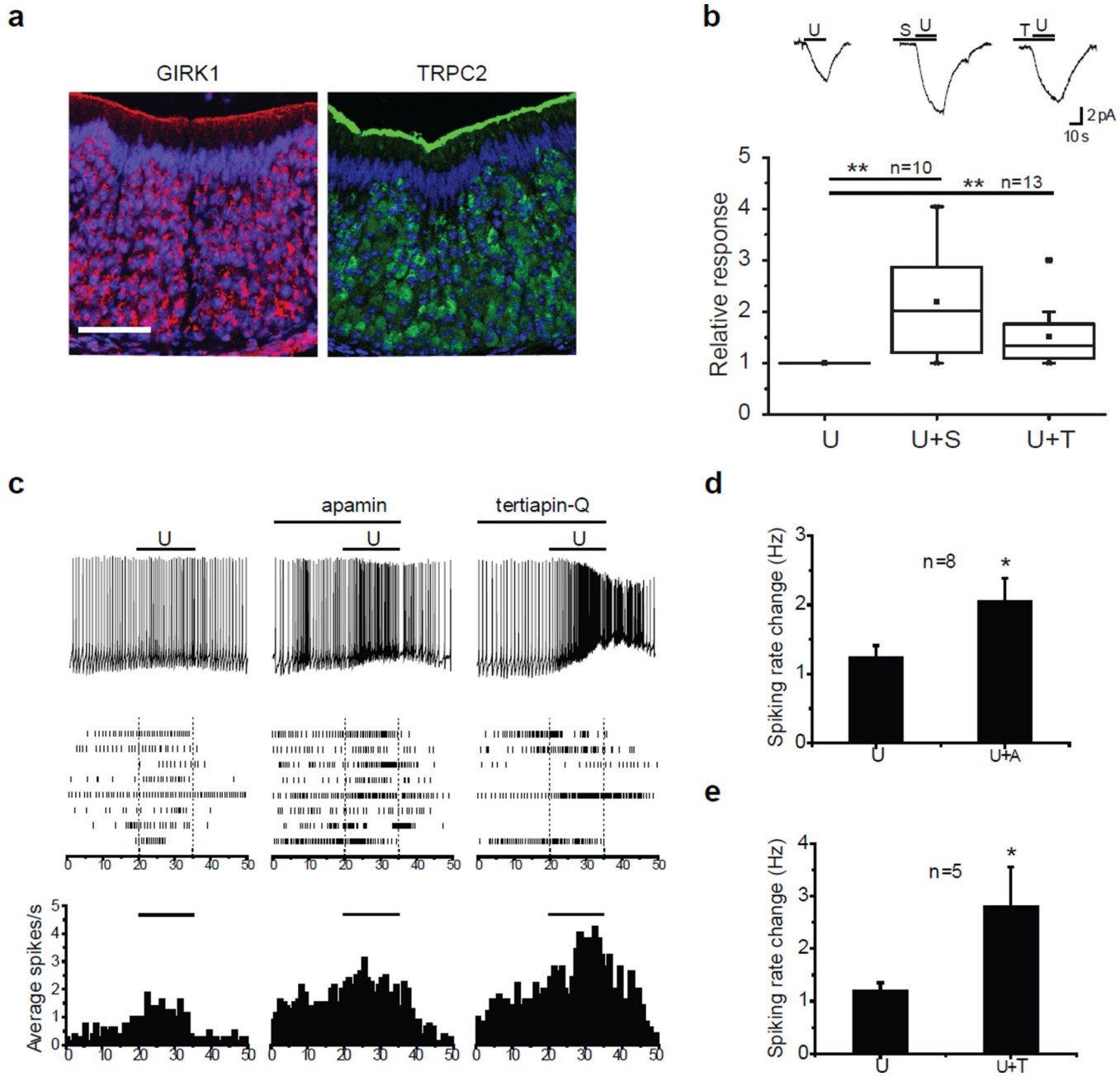

Fig. 3. Contribution of GIRK channels to VNO activation

(a) Immunofluorescent images of VNO sections stained with antibodies recognizing GIRK1 and TRPC2. Scale bar: 50 μm. **(b)** Sample traces and relative whole cell response to treatment with urine, urine with SCH23390 (S) or urine with tertiapin–Q (T). Box plot indicates relative current changes after treatment with SCH23390 ($U^{+}S$; 2.19 ± 0.32; n=10 cells) or tertiapin–Q ($U^{+}T$; 1.51 ± 0.15; n=13 cells). Bar graphs for current amplitude are presented in Supplementary Figs. 3a and b. All results are expressed as the mean ± SEM. ** indicates $p<0.01$ in Student's t–Test. **(c)** *top* : Sample traces of current clamp recordings of a VNO neuron in response to urine (left), urine with apamin (middle) and urine with tertiapin–Q (right). *middle* : Raster plots of the spiking activity of individual VNO neurons in

response to the treatments indicated in the top panel. Recordings in the same row are from the same cells. *bottom* : Peri–stimulus time histogram plots of average firing rates of neurons shown in the middle panel. **(d)** and **(e)** Bar graphs showing the changes in firing rate under the three conditions shown in **(c)**. * indicates $p < 0.05$ in Student's t–test.

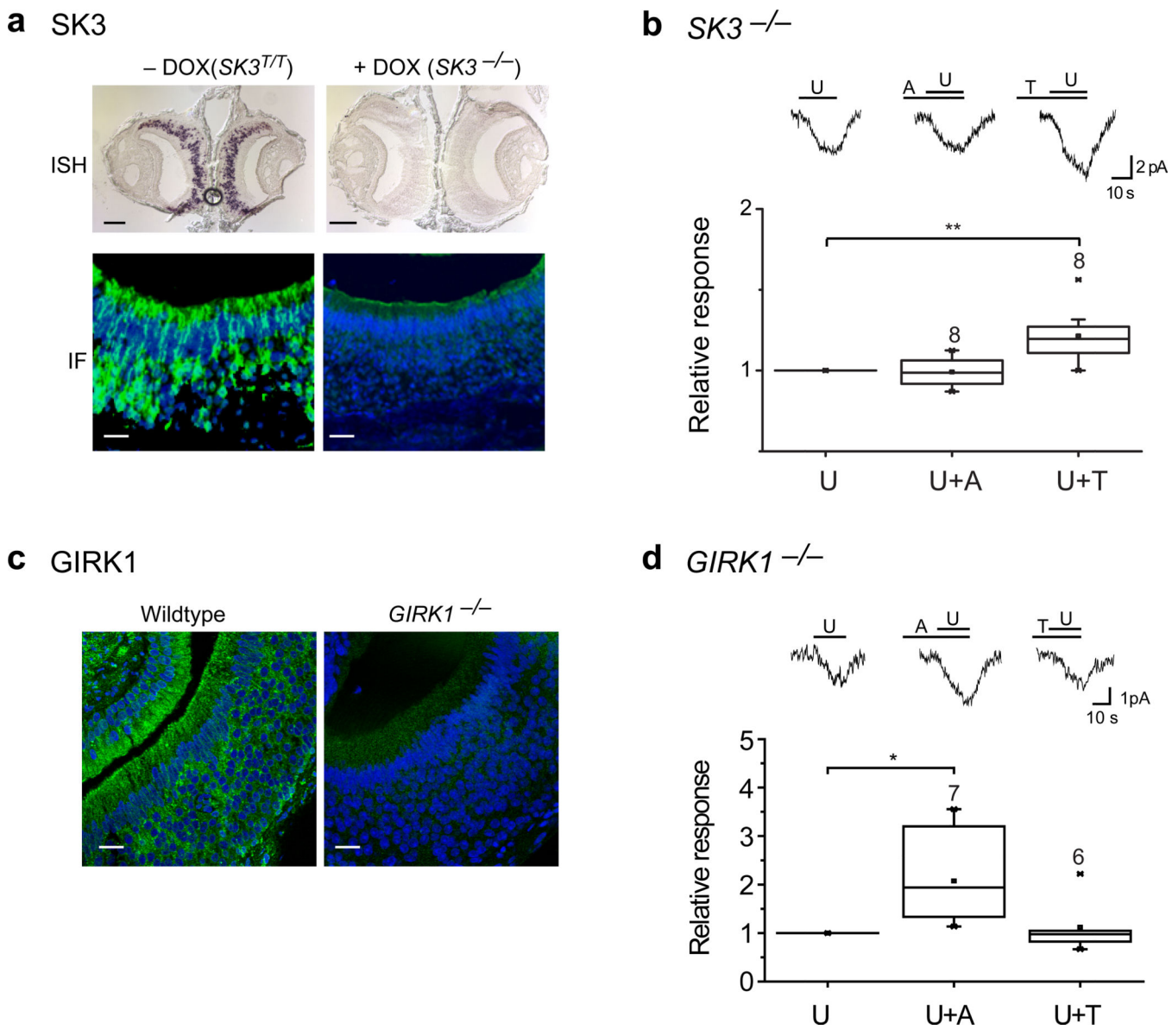

Fig. 4. Urine–evoked responses in *SK3*$^{-/-}$ and *GIRK1*$^{-/-}$ VNO neurons

(a) *In situ* hybridization (ISH) and immunofluorescent staining (IF) of SK3 in VNO sections from *SK3*$^{T/T}$ mice fed with or without doxycycline (DOX) diet. Scale bars: 100μm (top panels); 20μm (bottom panels). **(b)** Sample traces and box plot of relative whole cell response of *SK3*$^{-/-}$ VNO neuron to treatment with urine, urine with apamin (0.99 ± 0.03; n=8 cells) or urine with tertiapin–Q (1.21 ± 0.06; n=8 cells). Bar graphs for current amplitude are presented in Supplementary Figs. 4a and b. **(c)** Immunofluorescent staining of GIRK1 in wildtype and *GIRK1*$^{-/-}$ VNO. Scale bar: 20μm. **(d)** Sample traces and relative whole cell response of *GIRK1*$^{-/-}$ VNO neuron to treatment with urine, urine with apamin (2.07 ± 0.35; n=7) or urine with tertiapin–Q (1.11 ± 0.22; n=6). Bar graphs for current amplitude are presented in Supplementary Figs. 4c and d. * indicates p <0.05 and ** indicates p <0.01 in ANOVA. All results are expressed as the mean ± SEM.

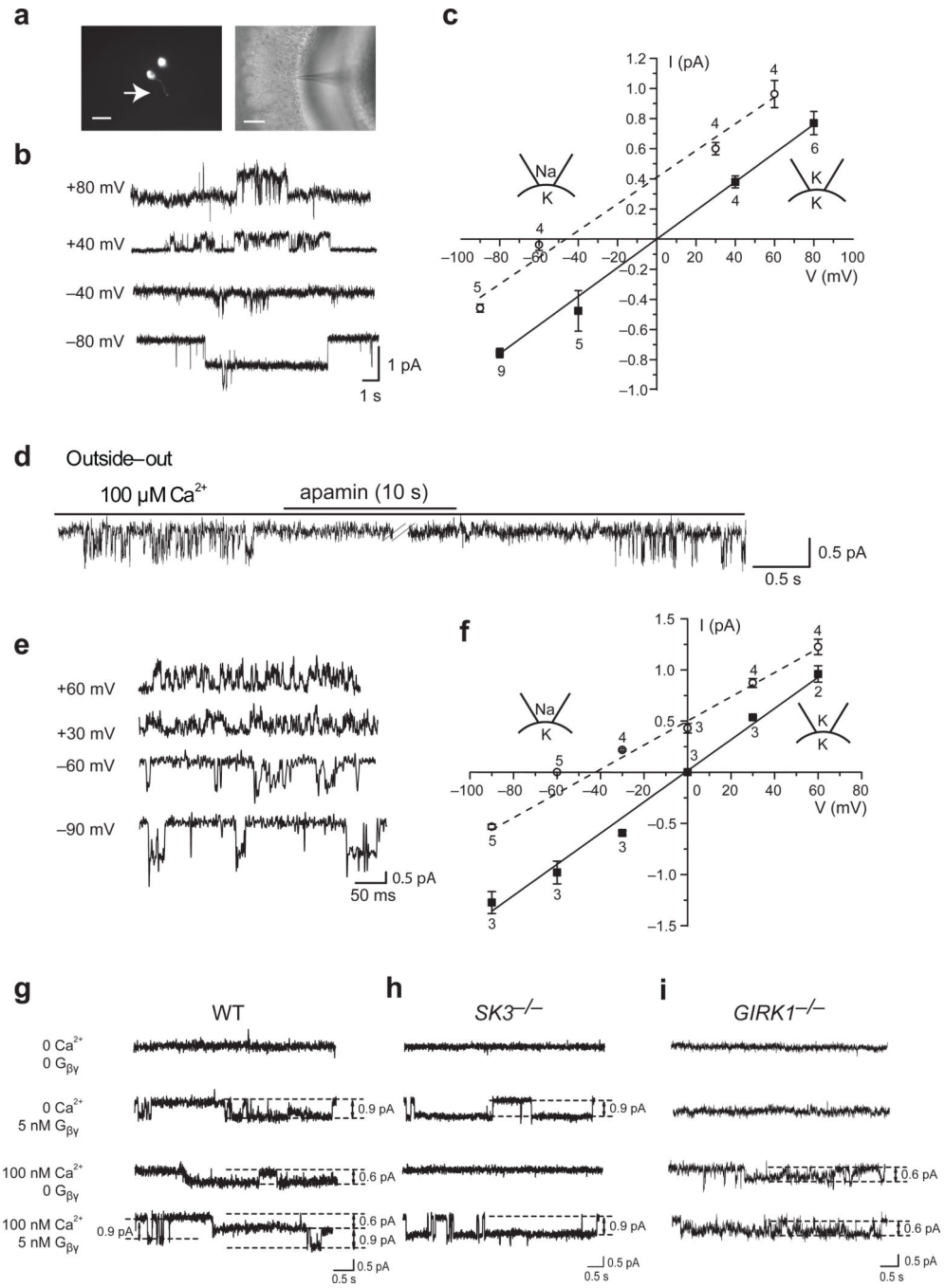

Fig. 5. Single channel activities in the VNO dendrite

(a) A fluorescent image of VNO neurons in the slice labeled with fluorescent dye (left) to show the dendritic knob (arrow) and a bright–field image of an electrode patching on neuronal dendrites in a VNO slice. Scale bars: 20μm (left) and 100μm (right).**(b)** Sample traces of single channel activities recorded from inside–out patches isolated from wildtype VNO dendrites. 100 μm Ca^{2+} was delivered to the intracellular side to evoke current. Holding potentials are labeled on the left of the traces. **(c)** I–V curve for Ca^{2+}–activated single channels. The currents are recorded under isotonic K^+ condition (solid squares fitted

with a solid line) or with extracellular K^+ replaced with Na^+ (open circle and dashed line). Numbers above each point indicate the number of patches used for analysis. **(d)** Single channel activity recorded from an outside–out patch isolated from a wildtype mouse. Short black line indicates the duration of 100 nM apamin application. **(e–f)** Single channel traces with holding potential from −90 mV to +60 mV **(e)** and the I–V curve (f) for $G_{\beta\gamma}$ evoked activities. **(g–i)** Single channel traces recorded from inside–out patches isolated from the VNO dendrites of wildtype **(g)**, *SK3*$^{-/-}$ **(h)** and *GIRK1*$^{-/-}$ **(i)** animals. Channel activities were recorded under four conditions. From top to bottom: 0 Ca^{2+}, no $G_{\beta\gamma}$; 0 Ca^{2+}, 5nM $G_{\beta\gamma}$; 100nM Ca^{2+}, no $G_{\beta\gamma}$; 100nM Ca^{2+}, 5nM $G_{\beta\gamma}$. Holding potential was −80 mV.

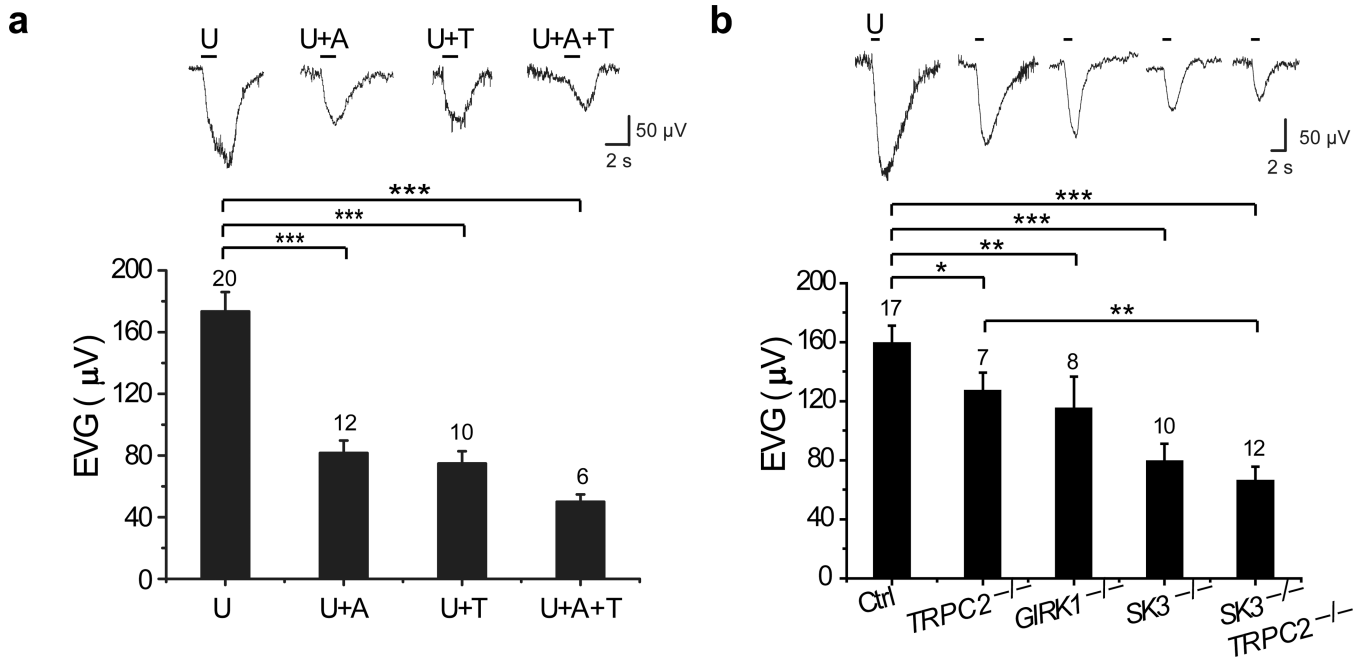

Fig. 6. SK3 and GIRK channels mediate urine–evoked inward current in intact preparations

(a) EVG sample traces and average responses to urine alone (173.42+/− 12.60, N=20), urine with apamin (A; 81.62 ± 8.06 μV, n=12), urine with tertiapin–Q (T; 74.8 ± 7.94 μV, n=10) and urine with apamin and tertiapin–Q (49.95± 4.79 μV; n=6). **(b)** EVG sample traces and average response from wildtype (159.40 ± 11.51 μV; n=17), *TRPC2*$^{-/-}$ (127.3 ± 11.93 μV; n=7), *GIRK1*$^{-/-}$ (115.21 ± 21.33 μV; n=8), *SK3*$^{-/-}$ (79.43 ± 11.68 μV; n=10) and SK3/TRPC2 double mutant (66.29 ± 9.17 μV; n=12). The numbers of recording are indicated. All results are expressed as the mean ± SEM. * indicates p <0.05 and ** indicates P <0.01 in ANOVA.

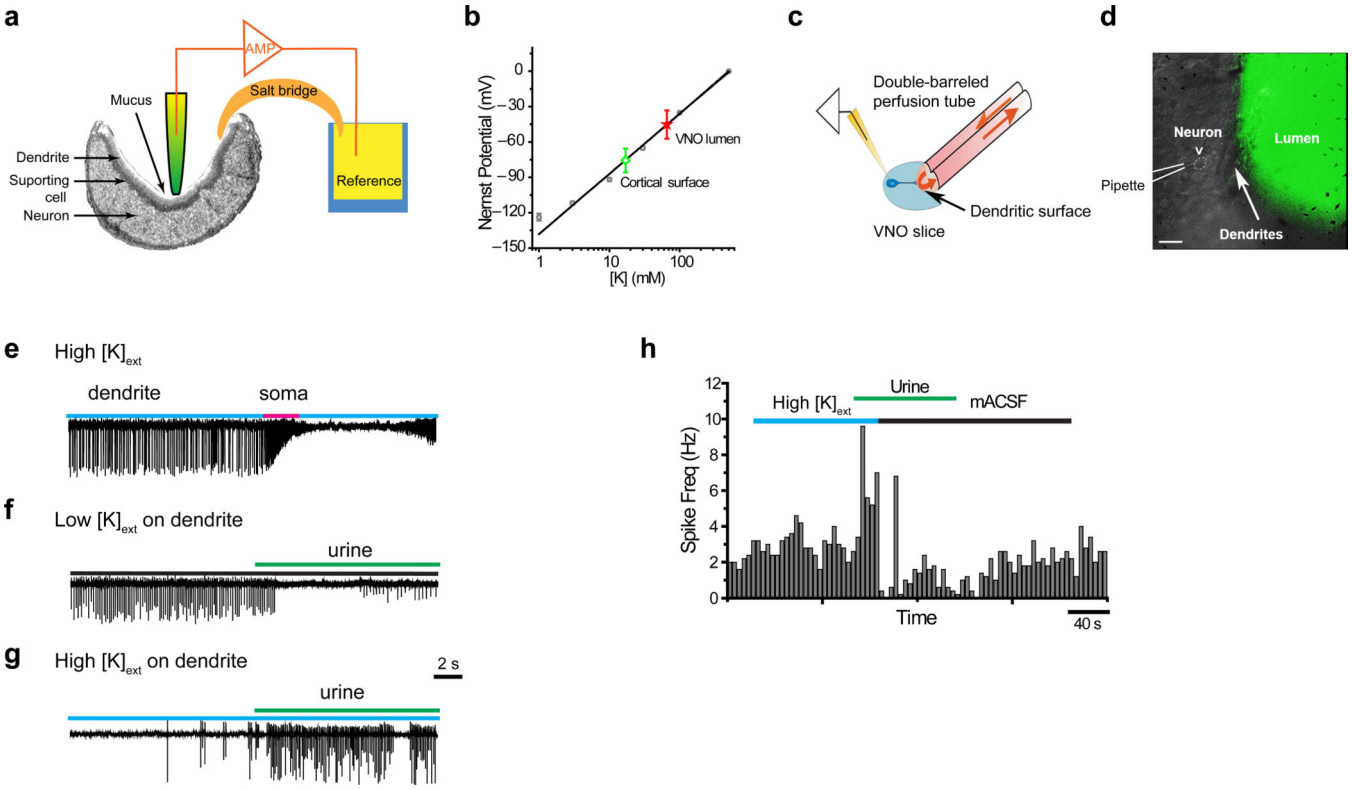

Fig. 7. High K^+ in the VNO lumen and reconstitution of native K^+ environment in VNO slices

(a) Illustration of the method for measuring K^+ concentration in VNO lumen using a K^+–selective electrode. **(b)** Nernst potential and extrapolated K^+ concentration for cortical surface (diamond; 17 ± 6 mM) and the VNO lumen (star; 66 ± 36 mM) are indicated on the standard curve produced from measuring a series of standard K^+ solutions. Six independent measurements are conducted. **(c)** Illustration of the local perfusion system with double–barreled perfusion tube. **(d)** Reconstitution of the lumen microenvironment. Fluorescein signal is used to indicate the diffusion range of the perfusate. Scale bar: 20μm. **(e–g)** Extracellular recording traces of the same VNO neuron in response to perfusion of urine with different concentrations of K^+. Vertical lines indicate individual spikes. **(e)** Response to pipette containing high K^+ solution moving from dendrite to soma and then back to dendrite. **(f)** Response to urine with low K^+ mACSF at the dendrite. **(g)** Response to urine with high K^+ solution at the dendrite. **(h)** Spiking rate of a different VNO neuron in response to urine application in high and low K^+ solutions perfused to the dendrite.

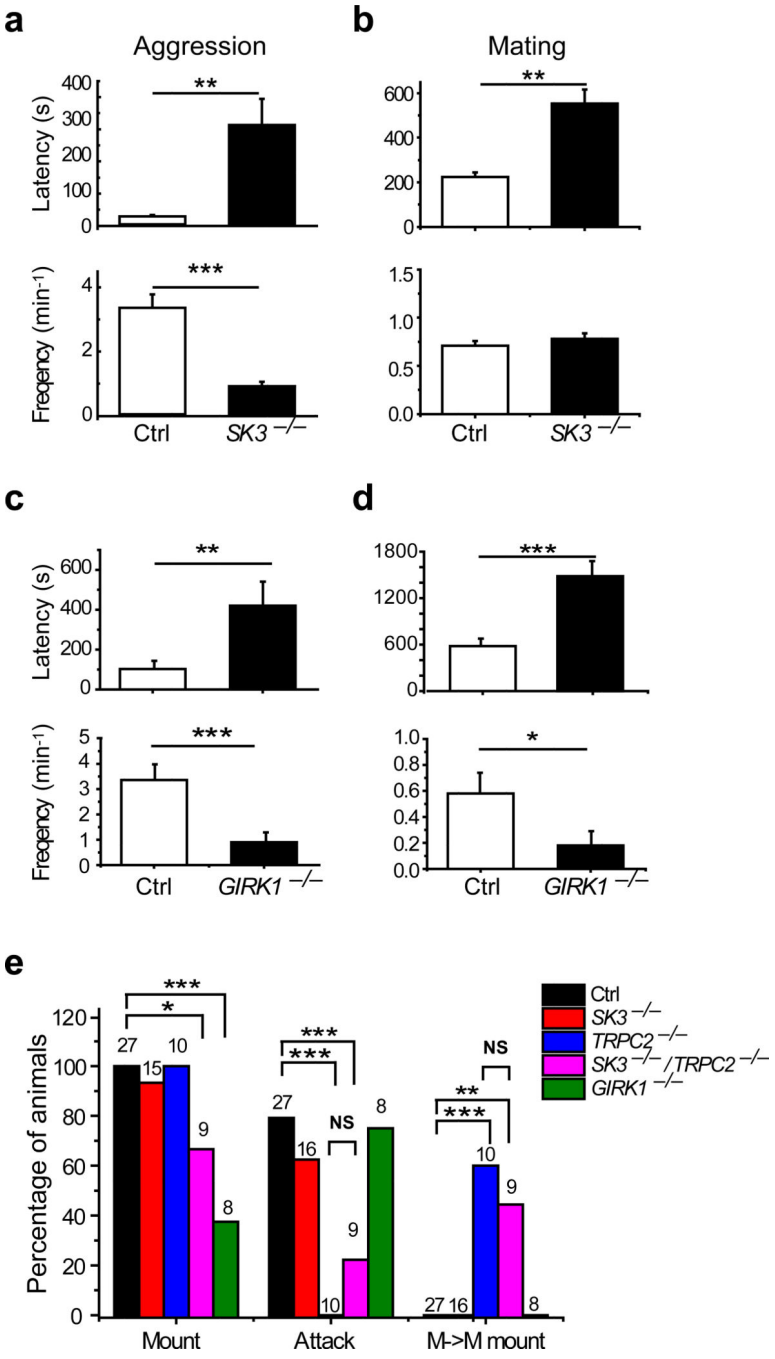

Fig. 8. Aggressive and mating behaviors in male *SK3*$^{-/-}$, *GIRK1*$^{-/-}$ and *TRPC2*$^{-/-}$ mice

(a and **c)** Average time of latency to first attack and the frequency of attacks for *SK3*$^{-/-}$ **(a)** and *GIRK1*$^{-/-}$ mice **(c)**. Controls for each groupare shown. **(b** and **d)** Average time of latency to first mount and the frequency of mounts for *SK3*$^{-/-}$ **(b)** and *GIRK1*$^{-/-}$ **(d)** mice. **(e)** Percentage of mice from each genotype displaying the following behaviors: male–to–female (M>F) mounting, male–to–male (M>M) attack and male–to–male (M>M) mounting. Total number of mice for each condition is indicated. * indicates p <0.05, ** indicates p

<0.01 and *** indicates p <0.001 in Student's t–test for **(a–d)** and in Fisher's Exact test for **(e)**.